Copper-Zinc Oxide Catalysts for Aldehyde Hydrogenation by Direct Reductive Activation of Precursors

Max Hiller[1,2] and Klaus Köhler[1,2,]*

Supporting Information available online

Bulk copper-zinc oxide hydrogenation catalysts are generally prepared by calcination of co-precipitated precursors followed by reduction. This study reports the direct reduction in hydrogen of co-precipitated oxy/hydroxy-carbonate precursors omitting calcination. Dried and incompletely calcined precursors are compared with calcined catalysts. The reduction reactions in hydrogen were monitored in situ by XRD and TGA-MS. Direct activation of precursors led to higher copper dispersions and increased catalytic activity in the hydrogenation of butyraldehyde to butanol as test reaction.

1 Introduction

Copper-Zinc (-Alumina) catalysts are well known for industrial scale methanol synthesis and water gas shift reaction (WGSR) [1–4]. Several literature reports are dealing with mechanistic investigations of the methanol synthesis and its active species [5–7]. The influence of synthesis conditions and structure-activity relationships are comprehensively investigated [5, 8–12]. The industrial scale catalyst is synthesized by a complex process starting with co-precipitation of soluble copper, zinc and aluminum salts (e.g., nitrates or chlorides), aging, drying, calcination, shaping, and (in situ) activation [9, 13–16].

Depending on the copper content, the precursor phase of typical Cu-Zn-Alumina methanol catalysts consists mainly of zincian-malachite ($(Cu,Zn)_2[(OH)_2|CO_3]$, obtained above 70 % Cu), and partially aurichalcite ($(Cu,Zn)_5[(OH)_6|(CO_3)_2]$, obtained below 50 % Cu). Additional phases like aluminum containing (Cu-)hydrotalcite ($Cu_6Al_2[(OH)_{16}|CO_3]\cdot4H_2O$), georgeite ($Cu_5(CO_3)_3$ $(OH)_4\cdot6H_2O$) and rosasite ($(Cu,Zn)_2[(OH)_2|CO_3]$) can be found too [11, 17]. For the aurichalcite precursor, a high temperature carbonate species ("HT-carbonate") can be obtained applying an incomplete calcination step. Calcination of aurichalcite between 250–300 °C leads to partial or complete formation of $(Cu,Zn)_5O_4(CO_3)$ depending on a variety of conditions (transport limitations, temperature ramp, etc.) [18]. A direct activation of the HT-carbonate to

copper-zinc oxide is possible. For methanol synthesis, inconsistent results regarding catalytic activity of directly activated HT-carbonate (i.e., without additional calcination to the oxides) can be found. While Baltes et al. report an increase in activity compared to completely calcined (oxide) catalysts, Schumann et al. report detrimental effects on the catalytic activity if phase pure HT-carbonates are used as catalyst precursor for the methanol synthesis [8, 19].

In addition to methanol synthesis, copper-zinc oxide catalysts (without alumina) are used in a variety of hydrogenation and hydrogenolysis reactions [20–25]. In comparison to the Cu-Zn-Al oxide methanol synthesis catalyst, fewer studies regarding the synthesis of the active phase, structure-activity relationships and mechanisms have been reported in literature. Investigations on the direct activation of non- or incompletely calcined samples for the gas phase hydrogenation, e.g., of aldehydes are rare and studies regarding the direct reductive activation of an aurichalcite precursor are missing so far [26].

[1]Max Hiller, Prof. Klaus Köhler
klaus.koehler@tum.de
Technical University of Munich, Department of Chemistry, Inorganic Chemistry, Lichtenbergstrasse 4, 85747 Garching, Germany.
[2]Max Hiller, Prof. Klaus Köhler
Technical University of Munich, Catalysis Research Center, Ernst-Otto- Fischer-Strasse 1, 85747 Garching, Germany.

This report focuses on the synthesis and catalytic properties of Cu-ZnO bulk catalysts (molar ratio Cu/Zn = 2:3) obtained by reductive activation of Cu-Zn (hydroxy-)carbonate precursors. The precursors were synthesized by co-precipitation followed by different thermal treatment resulting in different catalyst species. After co-precipitation and drying the hydroxycarbonate precursor is obtained. Incomplete calcination leads to the oxycarbonate species while full calcination yields the oxide species. The resulting catalysts were structurally characterized and the reaction pathways (reduction in hydrogen) and intermediates were investigated by in situ powder X-ray diffraction (p-XRD) and thermal analysis methods as a function of temperature and time. The activated catalysts were further tested in the hydrogenation model reaction of butyraldehyde to n-butanol.

2 Experimental

2.1 Synthesis

All precursors were prepared by co-precipitation of 0.4 M $Cu(NO_3)_2$ and 0.6 M $Zn(NO_3)_2$ in water with 1 M Na_2CO_3 as precipitation agent at controlled reaction conditions (copper/zinc ratio = 2:3, pH = 8, 60 min aging, 70 °C, Eq. (1)). The copper/zinc ratio was set according to preliminary catalysis tests resulting highest activity between 30–50 % copper loading (Supporting Information, Fig. S1). The solid was dried at 120 °C overnight (resulting in the hydroxycarbonate precursor). The HT-carbonate (oxycarbonate) was obtained by thermal treatment in air at 280 °C (5 K min^{-1}, 4 h)., and the calcined copper-zinc oxide at 350 °C (5 K min^{-1}, 4 h).

$$2Cu^{2+}(aq) + 3Zn^{2+}(aq) \xrightarrow[\substack{pH=8 \\ 70\ °C}]{1M\ Na_2CO_3} (Cu_2Zn_3)(OH)_6(CO_3)_2$$

(1)
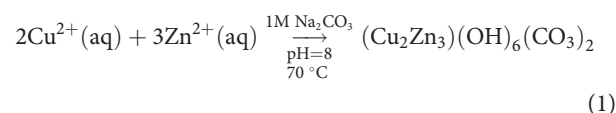
2.2 Characterization

Powder X-ray diffraction (p-XRD) was measured on an Empyrean Panalytical instrument (Cu Kα1, 0.013°/step, 50 s/step). For in situ measurements an Anton Paar XRK-900 reaction chamber connected to the XRD instrument was used (5 K min^{-1}, 10 mL min^{-1}, 2.5 % H$_2$/Ar). Particle sizes were determined by the Scherrer equation [27]. Elemental analysis was determined by an Agilent 700 ICP-OES. Samples were dissolved before in 6 M HCl.

A multiple element standard from Merck was used for calibration. For Cu determination wavelengths 324 and 327 nm were analyzed and 213 and 334 nm for Zn.

BET-surface areas were determined by N$_2$ adsorption on a Quantachrome 4XL at –196 °C. Samples were degassed at 120 °C in vacuum before measurement.

Temperature programmed reduction (TPR) and Cu-surface areas were measured on a Micromeritics Autochem II analyzer equipped with a thermal conductivity detector (TCD). TPR: 5 K min^{-1}, 50 mL min^{-1} 10 % H$_2$/Ar. Cu-surface area: Pre-reduction: 5 K min^{-1}, 250 °C, 1 h; 10 % H$_2$/Ar. Cu-surface area was determined by N$_2$O pulse-chemisorption [28, 29].

TGA-MS was measured on a Mettler-Toledo TGA/DSC 3+ coupled with a Pfeiffer GSD 320T gas analyzer. Calcination conditions: 10 K min^{-1}, 20 mL min^{-1} synthetic air. Reductive conditions: 5 K min^{-1}, 2.5 % H$_2$/Ar.

2.3 Catalytic Tests

The gas phase hydrogenation of butyraldehyde to n-butanol was performed in an 1/2″ stainless steel reactor with sieved catalyst (0.1–0.3 mm) placed in the isothermal zone of the reactor (Eq. (4)). The catalysts were pre-reduced in situ before catalysis (20 % H$_2$/N$_2$, $GHSV$ = 3000 h^{-1}, 2 K min^{-1}, 250 °C, 2 h). The hydrogenation was performed at 80–150 °C and 3.4 bar g. $GHSV$ was set to 18 000 h^{-1}, $LHSV$ to 4 h^{-1}. The temperature was controlled by a thermocouple in direct contact with the catalyst bed. Quantification was performed on an Agilent 7890 B equipped with an CP-Sil 5 column (25 m × 0.32 mm × 5 um). A sigmoidal curve-fit was used (Supporting Information, Tab. S1). The butyraldehyde conversion and the n-butanol selectivity was calculated as follows:

$$Conversion\ (\%) = \frac{mol\ of\ butyradelhyde\ converted}{mol\ of\ butyraldehyde\ fed}$$

(2)

$$Selectivity\ (\%) = \frac{mol\ of\ product}{mol\ of\ butyraldehyde\ converted}$$

(3)

(4)
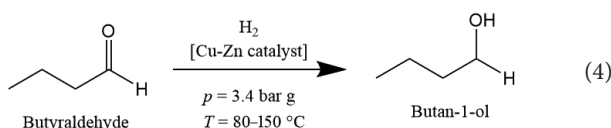
3 Results and Discussion

3.1 Synthesis of the Precursor and Characterization of the Pre-Catalysts after Varying Thermal Treatment

The catalysts were synthesized by classic co-precipitation at a controlled pH value of 8 (Eq. (1)). After precipitation and drying, a blue powder was obtained and analyzed by p-XRD. The main XRD reflexes belong to aurichalcite, $(Cu,Zn)_5(OH)_6(CO_3)_2$ (24.0, 30.9, 33.0, 34.3, 42.2, 57.5° 2θ) and hydrozincite, $(Zn)_5(OH)_6(CO_3)_2$ (13.2, 28.4, 30.5° 2θ) (Fig. 1). A quantification by Rietveld analysis yields an aurichalcite/hydrozincite ratio of 2:1 (Supporting Information, Fig. S7). Additionally, a minor amount of (Zn-)malachite
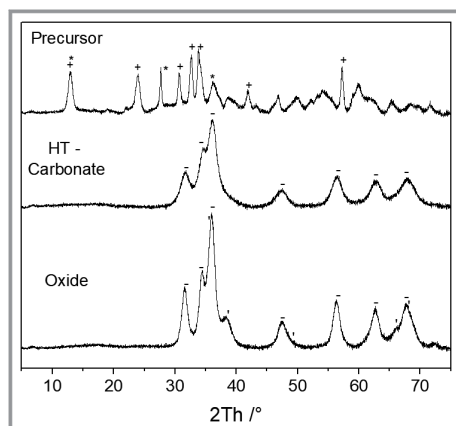
Figure 1. p-XRD of Precursor, HT-carbonate and Cu-Zn Oxide. Reflexes according to hydrozincite (*), aurichalcite (+), CuO ('), and ZnO (-) marked.
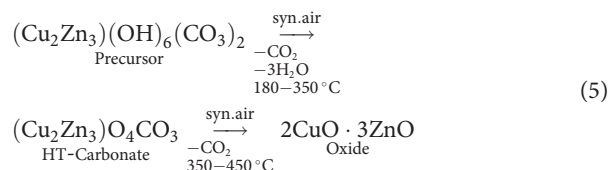
can be found [30, 31]. The total metal content of 62.4 % (determined by ICP-OES) agrees quite well with the calculated value for phase pure aurichalcite (61.2 %). The copper/zinc ratio of 1.9:3.1 fits the desired ratio of 2:3 (Tab. 1).

The HT-carbonate and the oxide species were obtained by partial or full calcination (see Experimental). After calcination at 280 °C, the powder XRD of the HT-carbonate contains reflexes belonging to ZnO (31.8, 34.3, 36.5, 47.5, 57.1, 63.2, 67.8° 2θ). No CuO or precursor phase can be found. The metal content fits with 73.2 % quite well to the theoretical value of the HT-carbonate species ($Cu_2Zn_3O_4CO_3$, 72.2 %) [18]. As expected, the copper:zinc ratio did not change. The mass loss of 14.2 % obtained during calcination is slightly below the expected value of 17.9% indicating minor residues of undecomposed precursor phase.

The full calcination at 350 °C resulted in a copper-zinc oxide catalyst. The oxide reflexes of ZnO and CuO (35.7, 49.2, 68.4° 2θ) are present [32, 33]. No additional reflexes could be found in the powder XRD. A quantification by Rietveld analysis yields 62 % ZnO and 38 % CuO (Supporting Information, Fig. S8). The total metal content determined by ICP-OES is with 76.0 % slightly below the theoretical value of 80.0 %. The copper/zinc ratio stays at 1.9:3.1 and fits exactly to the results obtained by Rietveld analysis. The weight loss during calcination fits with 25 % quite well

to the expected value of 26 %. In situ XRD investigations of the entire calcination process show a significant phase transformation between 250–275 °C (Supporting Information, Fig. S3).

The decomposition of the dried precursor was additionally monitored by TGA-MS (Fig. 2). Two peaks can be found during the decomposition process. In the first decomposition stage, a mass loss of 18 % was observed between 180–350 °C under release of CO_2 and H_2O. In the second decomposition stage, 7 % mass loss was detected between 350–450 °C releasing CO_2. No additional water is released, indicating an oxycarbonate phase after the first decomposition step. The intermediate species is known from literature as high temperature (HT-)carbonate with the formula $(Cu,Zn)_5O_4CO_3$ [18]. Although higher temperatures are needed to form the HT-carbonate in the temperature-programmed TGA experiment, it can be assumed that isothermal calcination at 280 °C also yields the pure oxycarbonate. Both the resulting metal content and weight loss during the calcination process agree well with the chemical formula of the HT-carbonate. A TGA experiment comparable to the calcination in the muffle furnace (isothermal step at 280 °C) yields a weight loss of 17 % (theoretical: 17.9 %) (Supporting Information, Fig. S2). A further increase in temperature leads to the complete decomposition of the oxycarbonate to form copper and zinc oxide (calcined catalyst, Eq. (5)).

$$\underset{\text{Precursor}}{(Cu_2Zn_3)(OH)_6(CO_3)_2} \xrightarrow[\substack{-CO_2 \\ -3H_2O \\ 180-350\,°C}]{syn.air}$$

$$\underset{\text{HT-Carbonate}}{(Cu_2Zn_3)O_4CO_3} \xrightarrow[\substack{-CO_2 \\ 350-450\,°C}]{syn.air} \underset{\text{Oxide}}{2CuO \cdot 3ZnO} \qquad (5)$$

In summary, both phase pure HT-carbonate and Cu-Zn oxide catalysts could be obtained by defined thermal treatment of the precursor phase, consisting mainly of aurichalcite and the Zn-pure hydrozincite. Those findings were supported by elemental analysis (ICP-OES) compared to the resulting mass loss during calcination. Additionally, TGA-MS experiments illustrate stepwise decomposition from precursor over HT-carbonate to the final oxide catalyst.

Table 1. Physical properties of aurichalcite, HT-carbonate and Oxide

Sample	Calc. T	Metal cont.[a]	n Cu/Zn	BET Surface	Cu Surface[b]	Cu Dispersion[b]	Cu^0 crys. size[c]	T_{max} TPR	Red. degree[d]	T_{50}
	[°C]	[wt %]	[–]	[m²g⁻¹]	[m²g⁻¹]	[%]	[nm]	[°C]	[%]	[°C]
Precursor	120	62.4	1.9:3.1	68	12	8.3	3.4	215	105	108
HT-carbonate	280	73.2	1.9:3.1	60	14	8.4	3.6	175	106	110
Oxide	350	76.0	1.9:3.1	48	10	5.8	5.8	160	100	115

[a] Elemental analysis, ICP-OES, [b] N_2O pulse-chemisorption, pre-reduction at 250 °C, [c] Scherrer equation [27], [d] TPR, TCD, 5 K min⁻¹, 10 % H_2/Ar.
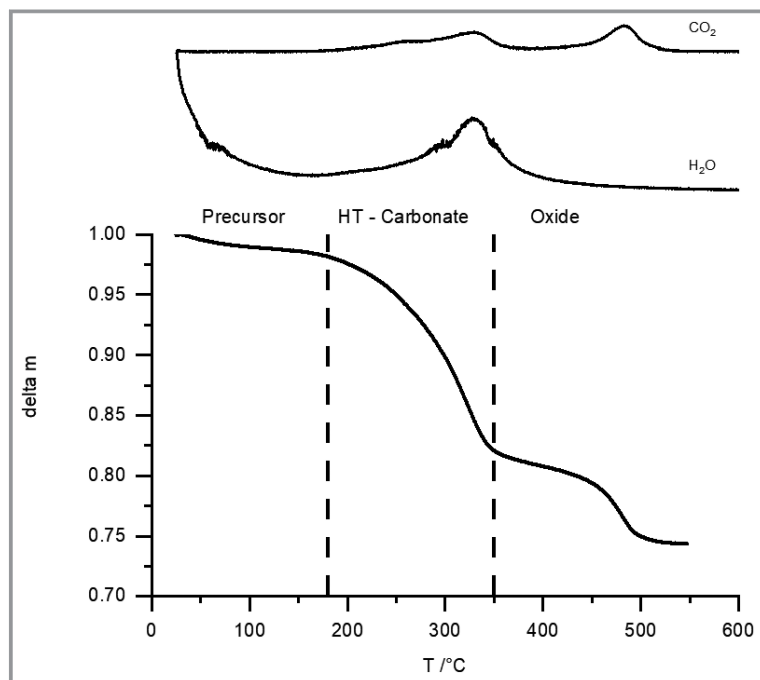
Figure 2. Thermogravimetric analysis of the decomposition of precursor to oxide phase. Experimental parameters: 10 K min^{-1}, syn. air.

3.2 Temperature-programmed Reduction and Characterization of the Reduced Catalysts

The three pre-catalysts (precursor, HT-carbonate and oxide) were characterized by temperature-programmed reduction (TPR), the total (BET) surface as well as the active metal (Cu) surface area after activation.

The TPR peaks of the dried precursor and the HT-carbonate are broader in comparison to the oxide peak. The peak maxima decrease with increasing thermal treatment: from 215 °C for the precursor to 175 °C for the HT-carbonate and 160 °C for the oxide (Fig. 3). The broader reduction peaks for both precursor and HT-carbonate could indicate a milder reduction progress. The reduction degree is above 100 % for both precursor and HT-carbonate (which can be explained by interference of the TCD signal with released CO_2 during the decomposition of precursor). The reduction degree of the fully calcined oxide pre-catalyst is 100 % indicating complete reduction of CuO to Cu.

The total surface area (BET) and active copper surface area (N_2O chemisorption) are higher for the dried precursor and the HT-carbonate compared to the calcined oxide catalyst (Tab. 1). The total surface area decreases with increasing calcination temperature. The dried precursor has a surface area of 68 m^{2}g^{-1} while the HT-carbonate has 60 m^{2}g^{-1}. The fully calcined oxide has the lowest surface area of 48 m^{2}g^{-1}. After reduction in hydrogen at 250 °C, the active Cu metal surface area is highest for the HT-carbonate (14 m^{2}g^{-1}) followed by the precursor (12 m^{2}g^{-1}) and the reduced oxide (10 m^{2}g^{-1}). Although the copper surface area

is higher for the HT-carbonate, the Cu dispersion is nearly the same for the precursor and the HT-carbonate (8.3 % and 8.4 %). The Cu dispersion of the oxide is significantly lower (5.8 %). The BET surface area decreases around 10 % while the copper dispersion stays nearly the same during the first partial calcination step (precursor to HT-carbonate). The complete calcination from precursor to the oxide results in a 30 % decrease of BET surface area and copper dispersion. This indicates a partial relation between BET surface area and copper dispersion. For Cu-Zn oxide catalysts a decrease of BET surface area at elevated calcination temperatures is known [34].

Summarizing the results reported so far, the following can be concluded: the variation of the thermal treatment resulted in three different catalyst variations. The precursor obtained after co-precipitation and drying consists of aurichalcite and hydrozincite, while the HT-carbonate formed after partial calcination represents a ZnO containing carbonate species (Fig. 1). Crystalline Cu-Zn oxide was obtained after full calcination at 350 °C (Fig. 2). The direct activation of both the dried precursor and the HT-carbonate is possible and can be advantageous (Fig. 3). Although slightly higher reduction temperatures are needed to reduce the precursor and the HT-carbonate, a higher copper dispersion as well as a higher total surface area is achieved in comparison to the fully calcined and subsequently reduced oxide catalyst (Tab. 1). In general, larger copper crystallites are obtained by reduction at higher temperature [35]. Potential explanations for the reverse observation in the present study are: (i) the copper-zinc inter-
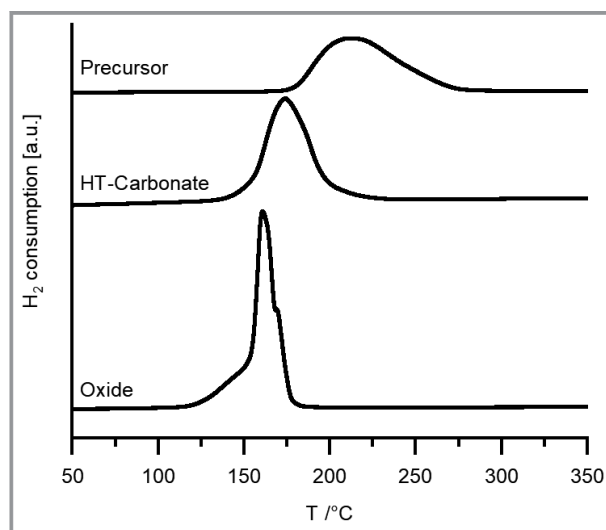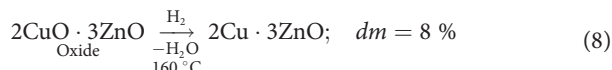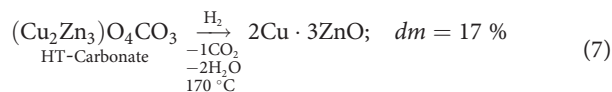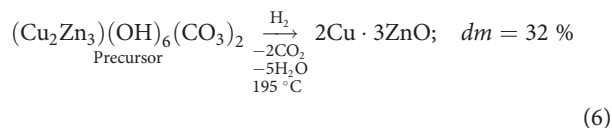

Figure 3. Temperature programmed reduction of un-/incompletely and fully calcined Cu-Zn catalysts. Experimental parameters and instrument: 5 K min^{-1}, 10 % H_2/Ar, Micromeritics Autochem II, TCD, –80 °C cooling trap.

action is stronger in the dried precursor and HT-carbonate and (ii) the reduction progress of these catalysts occurs over a broader temperature range (Fig. 3). It can be expected that potential hotspots during decomposition and reduction are prevented, decreasing the risk of sintering.

To get further information regarding the reduction process (formed intermediates, mechanism of reduction), both p-XRD and reductive TGA-MS measurements were performed in situ. First, the reduction processes of the three pre-catalysts were investigated by thermal gravimetric analysis coupled to a quadrupole mass spectrometer (TGA-MS) in flowing hydrogen (Fig. 4).

For the reduction of the dried precursor a mass loss of 32 % is found under release of H_2O and CO_2. No intermediate species can be detected during reduction at 195 °C. The HT-carbonate shows a mass loss of 17 % and also release of water and CO_2 at 170 °C. The fully calcined pre-catalyst (oxide) shows a mass loss of 7 % under release of water (no CO_2) at 160 °C. The mass loss and release of CO_2 for both dried precursor and HT-carbonate and water for all species indicate that both the reduction of copper(II) to metallic copper and the decomposition of residual precursor species (hydroxide/carbonate groups) take place simultaneously. The mass loss found by TGA measurements fits to model

calculations (Eq. (6)–(8)) and the temperature range fits well to the results of the TPR measurements.

$$\underset{\text{Precursor}}{(Cu_2Zn_3)(OH)_6(CO_3)_2} \xrightarrow[\substack{-2CO_2 \\ -5H_2O \\ 195\,°C}]{H_2} 2Cu \cdot 3ZnO; \quad dm = 32\,\% \tag{6}$$

$$\underset{\text{HT-Carbonate}}{(Cu_2Zn_3)O_4CO_3} \xrightarrow[\substack{-1CO_2 \\ -2H_2O \\ 170\,°C}]{H_2} 2Cu \cdot 3ZnO; \quad dm = 17\,\% \tag{7}$$

$$\underset{\text{Oxide}}{2CuO \cdot 3ZnO} \xrightarrow[\substack{-H_2O \\ 160\,°C}]{H_2} 2Cu \cdot 3ZnO; \quad dm = 8\,\% \tag{8}$$

To get further insights into the activation, the reduction of precursor, HT-carbonate and oxide was also monitored by in situ X-ray powder diffraction under reductive atmosphere (Fig. 5).

For the dried precursor, reflexes belonging to aurichalcite and hydrozincite are present at room temperature. No notable phase transformation is found up to 200 °C. At 250 °C, a phase transformation directly to zinc oxide and metallic copper is observed. For the HT-carbonate mainly reflexes belonging to zinc oxide and minor reflexes of remaining precursor phase can be found at room temperature. The latter ones could be detected due to a higher resolution compared to the standard p-XRD measurements at room temperature (Supporting Information, Fig. S5). This indicates minor residues of the hydroxycarbonate phase. No notable phase transformation is observed up to 175 °C. At 200 °C only reflexes belonging to metallic copper and zinc oxide are detected. The Cu-crystallite size does not change significantly between 200–250 °C. For the fully calcined oxide catalyst, the phase transformation from copper oxide to metallic copper takes place between 175–200 °C. At room temperature and up to 175 °C, reflexes belonging to both copper and zinc oxide are detected. Above 175 °C only metallic copper is found. The Cu(0) reflex at 43.3° 2θ is narrower compared to both reduced precursor and HT-carbonate (additional in situ XRD pattern in Supporting Information, Figs. S4–S6). The copper
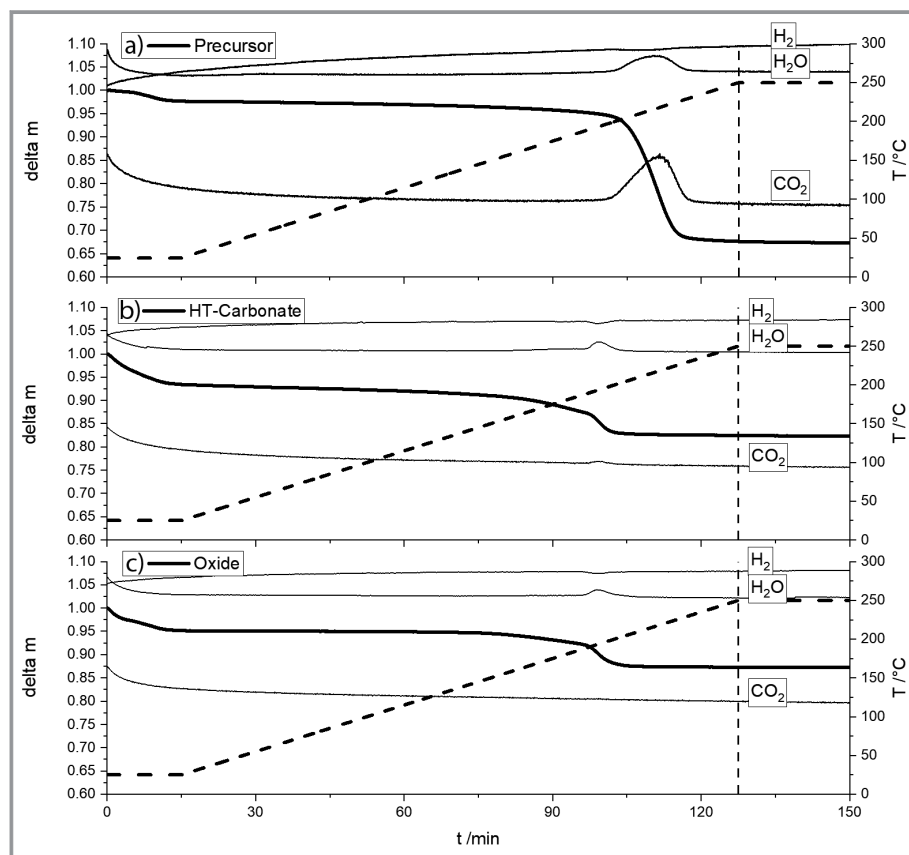
Figure 4. Reductive TGA of a) Precursor, b) HT-carbonate, and c) oxide. Experimental parameters: 5 K min⁻¹, 20 mL min⁻¹ 2.5 % H_2/Ar. Thick solid line represents the mass loss (left *y*-axis), thick dashed line the temperature (right *y*-axis) and thin solid lines the consumption of H_2 respectively evolution H_2O and CO_2.
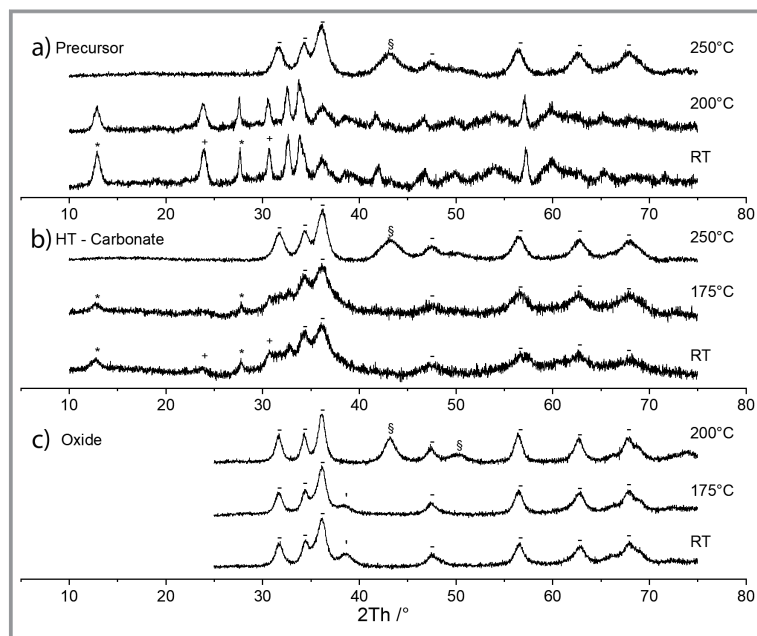
Figure 5. Reduction of a) Precursor, b) HT-carbonate, and c) Oxide to Cu/ZnO. Reflexes of hydrozincite (*), aurichalcite (+), CuO ('), Cu (§), and ZnO (-) marked. Experimental parameters: 5 K min^{-1}, 10 mL min^{-1}, 2.5 % H$_2$/Ar.

crystallite size was determined by Scherrer equation to be 3.4 respectively 3.6 nm for the reduced precursor/HT-carbonate compared to 5.8 nm for the reduced oxide. The copper particle size of the directly reduced precursor and HT-carbonate is roughly 40 % smaller compared to the completely calcined and subsequently reduced oxide. This agrees with the decrease in dispersion of the oxide species compared to the precursor/HT-carbonate.

These complementary in situ studies confirmed that reductive activation starting from different pre-catalysts yields the completely reduced Cu/ZnO catalyst in all cases (Eq. (6)–(8)). The decomposition of hydroxide and carbonate (precursors) and the reduction of copper take place at the same time (Figs. 4 and 5). No (crystalline) intermediates as, e.g., oxidic state were found. An increased calcination temperature of the pre-catalyst results in slightly lower reduction temperature but also larger copper crystallites and lower copper dispersions.

3.4 Catalysis

The three samples were tested in the gas phase hydrogenation of butyraldehyde to *n*-butanol after in situ activation (Eq. (4)). The activities of the reduced precursor and the reduced HT-carbonate are higher compared to the activated oxide after calcination (Fig. 6 and Tab. S1). For the precursor and the HT-carbonate reaction rates of 54 respectively 52 mmol h^{-1}g$_{Kat}^{-1}$ *n*-butanol are obtained, while the completely calcined and reduced catalyst shows a rate of 45 mmol h^{-1}g$_{Kat}^{-1}$ at 130 °C. The selectivity to *n*-butanol is

for all samples > 99.5 %, only minor side products like 2-ethyl-2-hexenal and butyl butyrate are found. The selectivity was 99.8 % both for the oxide and the HT-carbonate compared to 99.7 % for the precursor (measured at full conversion). In general, the selectivity is not affected by the calcination temperature. The T_{50} values increase from 108 °C (precursor) over 110 °C (HT-carbonate) to 115 °C for the oxide. Full conversion is reached at 145 °C for the activated precursor, 150 °C for the activated HT-carbonate and 165 °C for the oxide. The modified thermal treatment (no or incomplete calcination) of the catalyst precursor does not only lead to higher copper dispersion but also to enhanced catalytic performance.

4 Conclusions

The control of the thermal treatment of co-precipitated Cu-Zn precursors allows for the targeted synthesis of any of the three described catalyst phases: Bulk copper-zinc oxide hydrogenation catalysts can be prepared by reductive activation after full calcination to the Cu/Zn metal oxides. Additionally, the direct reduction of both precursor and partially calcined HT-carbonate in hydrogen yields an active hydrogenation catalyst. The direct activation of the dried or incompletely calcined precursors leads to a higher copper dispersion and increased catalytic activity in the hydrogenation of butyraldehyde to *n*-butanol compared to the activated oxide catalyst. The copper reduction takes place at the same time as the decomposition of the (hydroxy-)carbonate phases without formation of (crystalline) CuO/ZnO oxide intermediates.
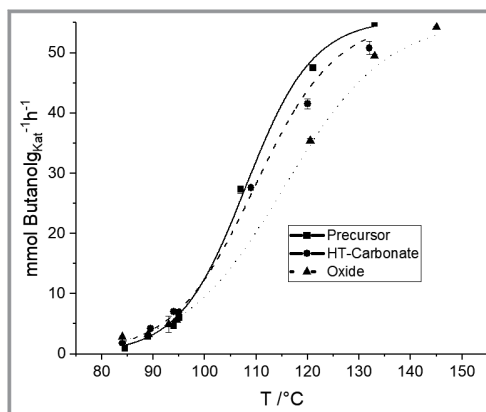
Figure 6. Hydrogenation of butyraldehyde to *n*-butanol. Experimental parameters: 3.4 bar g, *GHSV* = 18 000 h^{-1}, *LHSV* = 4 h^{-1}, quantification on an Agilent 7890B equipped with an CP-Sil column. Sigmoidal curve fit.

Supporting Information

Symbols used

dm	[%]	delta mass
$GHSV$	[h^{-1}]	gas hourly space velocity
$LHSV$	[h^{-1}]	liquid hourly space velocity
T	[°C]	Temperature

Abbreviations

BET	Brunauer–Emmett–Teller (theory)
HT-carbonate	high-temperature carbonate phase
ICP-OES	inductively coupled plasma optical emission spectrometry
p-XRD	powder X-ray diffraction
RT	room temperature
TCD	thermal conductivity detector
TGA-MS	thermogravimetric analysis–mass spectrometry
TPR	temperature-programmed reduction
WGS	water gas shift

References

[1] J. C. J. Bart, R. P. A. Sneeden, *Catal. Today* **1987**, *2 (1)*, 1–124. DOI: https://doi.org/10.1016/0920-5861(87)80001-9

[2] W. Fu, Z. Bao, W. Ding, K. Chou, Q. Li, *Catal. Commun.* **2011**, *12 (6)*, 505–509. DOI: https://doi.org/10.1016/j.catcom.2010.11.017

[3] X. Jiang, X. Nie, X. Guo, C. Song, J. G. Chen, *Chem. Rev.* **2020**, *120 (15)*, 7984–8034. DOI: https://doi.org/10.1021/acs.chemrev.9b00723

[4] M. D. Porosoff, B. Yan, J. G. Chen, *Energy Environ. Sci.* **2016**, *9 (1)*, 62–73. DOI: https://doi.org/10.1039/c5ee02657a

[5] J. D. Grunwaldt, A. M. Molenbroek, N. Y. Topsøe, H. Topsøe, B. S. Clausen, *J. Catal.* **2000**, *194 (2)*, 452–460. DOI: https://doi.org/10.1006/jcat.2000.2930

[6] T. Lunkenbein, J. Schumann, M. Behrens, R. Schlogl, M. G. Willinger, *Angew. Chem. Int. Ed.* **2015**, *54 (15)*, 4544–4548. DOI: https://doi.org/10.1002/anie.201411581

[7] M. S. Spencer, *Top. Catal.* **1999**, *8*, 259. DOI: https://doi.org/10.1023/a:1019181715731

[8] C. Baltes, S. Vukojevic, F. Schuth, *J. Catal.* **2008**, *258 (2)*, 334–344. DOI: https://doi.org/10.1016/j.jcat.2008.07.004

[9] M. Behrens, F. Girgsdies, A. Trunschke, R. Schlögl, *Eur. J. Inorg. Chem.* **2009**, *2009 (10)*, 1347–1357. DOI: https://doi.org/10.1002/ejic.200801216

[10] P. Porta, *J. Catal.* **1988**, *109 (2)*, 367–377. DOI: https://doi.org/10.1016/0021-9517(88)90219-9

[11] J. L. Li, T. Inui, *Appl. Catal. A* **1996**, *137 (1)*, 105–117. DOI: https://doi.org/10.1016/0926-860x(95)00284-7

[12] P. Kowalik, M. Konkol, M. Kondracka, W. Próchniak, R. Bicki, P. Wiercioch, *Appl. Catal. A* **2013**, *452*, 139–146. DOI: https://doi.org/10.1016/j.apcata.2012.11.019

[13] J. W. Couves et al., *Nature* **1991**, *354*, 465–468. DOI: https://doi.org/10.1038/354465a0

[14] D. Guse, S. Polierer, S. Wild, S. Pitter, M. Kind, *Chem. Ing. Tech.* **2022**, *94 (3)*, 314–327. DOI: https://doi.org/10.1002/cite.202100197

[15] S.-I. Fujita, S. Moribe, Y. Kanamori, M. Kakudate, N. Takezawa, *Appl. Catal. A* **2001**, *207 (1–2)*, 121–128. DOI: https://doi.org/10.1016/s0926-860x(00)00616-5

[16] G. Moretti, G. Ferraris, G. Fierro, M. Lo Jacono, *Surf. Interface Anal.* **2006**, *38 (4)*, 224–228. DOI: https://doi.org/10.1002/sia.2129

[17] G. Simson, E. Prasetyo, S. Reiner, O. Hinrichsen, *Appl. Catal. A* **2013**, *450*, 1–12. DOI: https://doi.org/10.1016/j.apcata.2012.06.040

[18] A. Tarasov, J. Schumann, F. Girgsdies, N. Thomas, M. Behrens, *Thermochim. Acta* **2014**, *591*, 1–9. DOI: https://doi.org/10.1016/j.tca.2014.04.025

[19] J. Schumann, A. Tarasov, N. Thomas, R. Schlögl, M. Behrens, *Appl. Catal. A* **2016**, *516*, 117–126. DOI: https://doi.org/10.1016/j.apcata.2016.01.037

[20] C. Dörfelt et al., *J. Catal.* **2021**, *395*, 80–90. DOI: https://doi.org/10.1016/j.jcat.2020.12.017

[21] C. P. Jiménez-Gómez et al., *J. Catal.* **2016**, *336*, 107–115. DOI: https://doi.org/10.1016/j.jcat.2016.01.012

[22] V. Pospelova, J. Aubrecht, O. Kikhtyanin, K. Pacultová, D. Kubička, *ChemCatChem* **2019**, *11 (8)*, 2169–2178. DOI: https://doi.org/10.1002/cctc.201900334

[23] X. Yang, X. Xiang, H. Chen, H. Zheng, Y.-W. Li, Y. Zhu, *ChemCatChem* **2017**, *9 (15)*, 3023–3030. DOI: https://doi.org/10.1002/cctc.201700279

[24] V. Pospelova, J. Aubrecht, K. Pacultová, M. Lhotka, O. Kikhtyanin, D. Kubička, *Catal. Sci. Technol.* **2020**, *10 (10)*, 3303–3314. DOI: https://doi.org/10.1039/d0cy00143k

[25] V. Pospelova, J. Aubrecht, O. Kikhtyanin, D. Kubička, *Appl. Catal. A* **2021**, *624*, 118320. DOI: https://doi.org/10.1016/j.apcata.2021.118320

[26] E. L. Rodrigues, A. J. Marchi, C. R. Apesteguia, J. M. C. Bueno, *Appl. Catal. A* **2005**, *294 (2)*, 197–207. DOI: https://doi.org/10.1016/j.apcata.2005.07.029

[27] P. Scherrer, *Nachr. Ges. Wiss. Göttingen, Math.-Phys. Klasse* **1918**, *1918*, 3.

[28] O. Hinrichsen, T. Genger, M. Muhler, *Chem. Eng. Technol.* **2000**, *23 (11)*, 956–959. DOI: https://doi.org/10.1002/1521-4125(200011)23:11<956::AID-CEAT956>3.0.CO;2-L

[29] D. A. M. Monti, A. Baiker, *J. Catal.* **1983**, *83 (2)*, 323–335. DOI: https://doi.org/10.1016/0021-9517(83)90058-1

[30] L. G. Berry, *Am. Mineral.* **1951**, *36 (5–6)*, 484–503.

[31] J. L. Jambor, G. Pouliot, *Can. Mineral.* **1965**, *8 (3)*, 385–389.

[32] J. I. Langford, D. Louër, *J. Appl. Crystallogr.* **1991**, *24 (2)*, 149–155. DOI: https://doi.org/10.1107/S0021889890012092

[33] J. D. Hanawalt, H. W. Rinn, L. K. Frevel, *Ind. Eng. Chem. Anal. Ed.* **1938**, *10 (9)*, 457–512. DOI: https://doi.org/10.1021/ac50125a001

[34] J. Yang et al., *Catal. Commun.* **2004**, *5 (9)*, 505–510. DOI: https://doi.org/10.1016/j.catcom.2004.06.005

[35] F. Jiang et al., *Catal. Sci. Technol.* **2022**, *12 (2)*, 551–564. DOI: https://doi.org/10.1039/d1cy01836a